Stress, Distance, Magnitude, and Clustering Influences on the Success or Failure of an Aftershock Forecast: The 2013 M 6.6 Lushan Earthquake and Other Examples

by Tom Parsons and Margaret Segou

INTRODUCTION

Immediately after the 12 May 2008 M 7.9 Wenchuan earthquake, we began calculating the static stress change on major faults surrounding the rupture zone (Parsons *et al.*, 2008), and Toda *et al.* (2008) mapped out regional Coulomb stress changes (Fig. 1). The purpose was twofold: (1) to identify the most likely locations (stress increases) of dangerous aftershocks, and (2) to conduct a prospective test of stress mapping as a rapid-response forecast tool. The occurrence of the 20 April 2013 M 6.6 Lushan earthquake in the Longmen fault zone near Ya'an was consistent with the prospective static stress forecast; for example, press coverage in 2008 (Kuang, 2008) stated

> *According to their results, published in Nature on 6 July, Ya'an Thrust, Xiong Po Thrust, and Xianshuihe Fault, all near Longmen Fault where the earthquake occurred, show a notable increase in static stress changes, and therefore face a high risk of aftershocks.*
>
> *"The 12 May earthquake ... caused grievous losses, yet its legacy includes possible large aftershocks in the near future because it increased failure stress on important faults within and around the Sichuan basin," write the authors.*

However, a formal evaluation of the post-Wenchuan forecast performance by Parsons *et al.* (2012) was not favorable, as

> *...we show two fully prospective static stress forecasts that have failed to reproduce spatial patterns of microseismicity ... over a span of 1 to 4 years we find that forecast spatial distributions of earthquakes are violated, with clear rate increases in stable stress-shadowed zones at Kashmir, and at Wenchuan.*

Indeed, a visual examination of Figure 1 shows many examples of aftershocks occurring at high rates in stress-shadow (calculated decrease) areas where a decrease in seismicity rate would have been expected.

The 2013 Lushan earthquake caused 203 deaths, injured at least 11,492, and affected more than 1.5 million others (UNICEF China, 2013). We consider the Lushan event as an aftershock of the 2008 Wenchuan mainshock per Scholz (2002), who defines them as

> *Aftershocks typically begin immediately following the mainshock over the entire rupture area and its surroundings, although they are commonly concentrated in locations where one might expect large stress concentrations to have been produced by the mainshock rupture.*

Additionally, Parsons (2002) cataloged thousands of $M > 5$ stress-triggered earthquakes that occurred up to 240 km

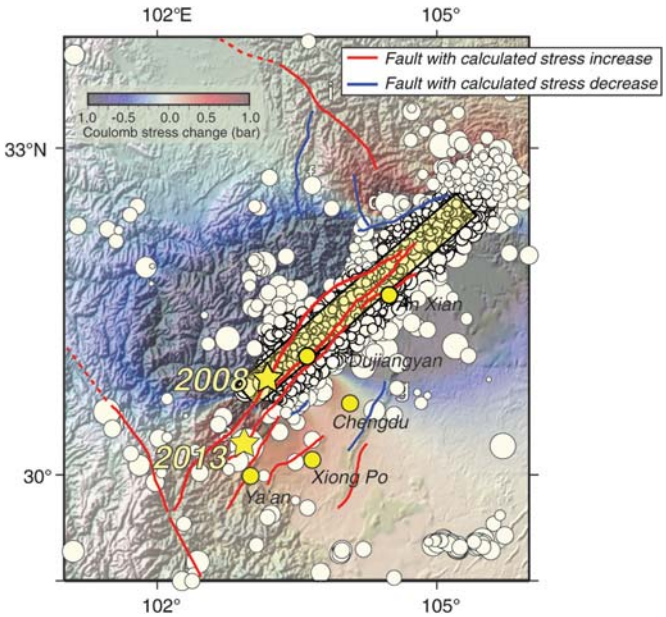

▲ **Figure 1.** Earthquake activity ($M \geq 2$) following the 12 May 2008 M 7.9 Wenchuan mainshock in Sichuan Province, China. Epicenters are superimposed on static stress-change calculations made shortly after the mainshock in 2008 on mapped faults (red and blue lines) and optimally oriented faults (Parsons *et al.*, 2008). It is evident that many aftershocks occurred in regions and faults with calculated stress decreases, which led Parsons *et al.* (2012) to conclude that the forecast was a failure.

doi: 10.1785/0220130100

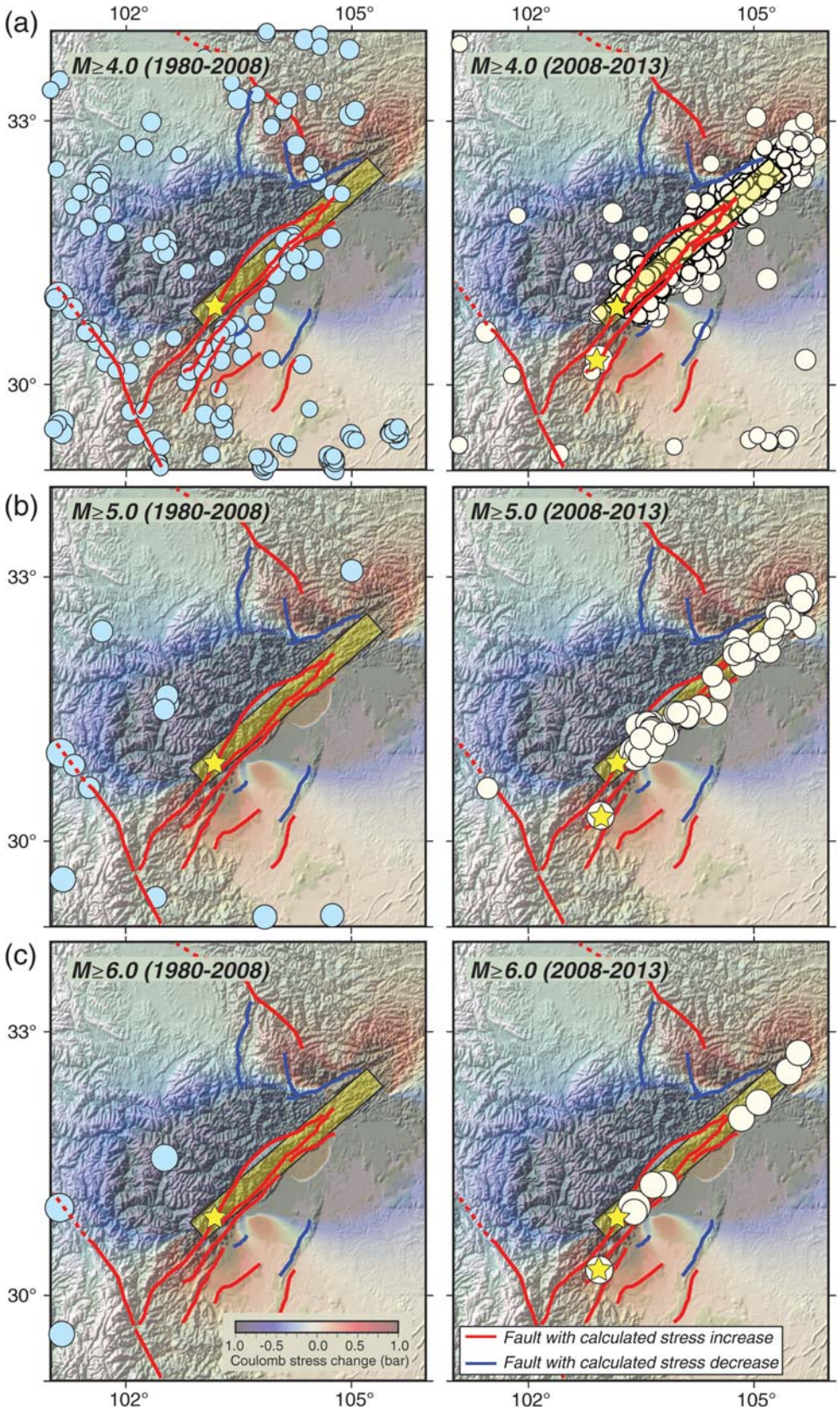

▲ **Figure 2.** Earthquake activity for (a–c) different magnitude thresholds shown (left column) before and (right column) after the 12 May 2008 *M* 7.9 Wenchuan mainshock. Blue dots represent 1980–2008 events, whereas yellow are 2008–present events. The same stress-change patterns are shown as in Figure 1. As lower magnitude events are excluded, the fit to stress-change patterns improves. The highest magnitude events are only found near the mainshock rupture (approximated by the yellow rectangle).

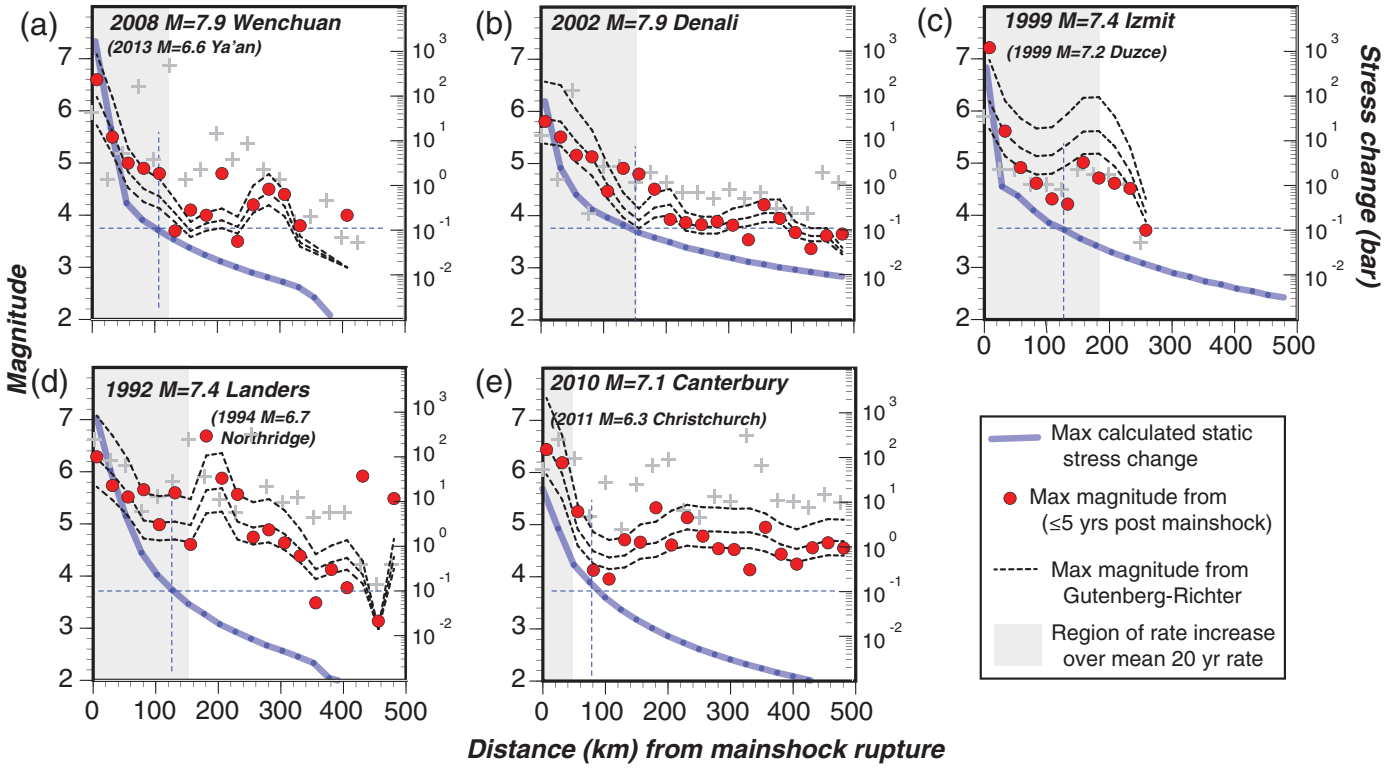

▲ **Figure 3.** Maximum observed earthquake magnitude (red dots) versus distance from rupture surface for a group of $M \geq 7$ continental earthquakes. The dashed black lines show calculated expected maximum magnitude versus distance, as extrapolated from Gutenberg–Richter relations with *b*-values ranging from 0.8 to 1.2. The heavy blue lines show calculated maximum Coulomb stress change versus distance. The gray-shaded regions show approximate extents of the calculated earthquake rate increase above the 20 year means. The horizontal dashed blue line shows the +0.1 bar stress-change threshold, and the vertical dashed blue line marks the distance from the mainshock planes where that occurs, which tends to be located fairly close to the earthquake rate-increase threshold. Gray plus symbols show maximum observed magnitudes versus distance that occurred in the 20-year periods before mainshocks.

away from mainshock ruptures and behaved like aftershocks with Omori-law temporal decays that persisted for 7–11 years after the mainshocks in a global study.

Where and when the 2013 M 6.6 Lushan earthquake occurred raises two key questions: (1) Are static stress-change calculations more applicable to larger aftershocks? (2) Are empirical forecasts (those based on observed activity levels and known temporal and spatial aftershock behaviors) always better than stress-based methods? A single case such as the Wenchuan–Lushan pairing is not necessarily representative, so we look at additional large continental earthquakes and their aftershock relationships.

AFTERSHOCK DISTRIBUTION OF THE 2008 *M* 7.9 WENCHUAN EARTHQUAKE

As is typical following a large earthquake, the spatial distribution of seismicity was strongly altered by the 2008 M 7.9 Wenchuan event (Fig. 2). The highest magnitude aftershocks are located closest to the mainshock rupture and are consistent with calculated Coulomb stress change calculations. There are many aftershocks of $M \geq 4.0$ that occurred in the calculated stress shadow regions (Fig. 2a); however, when the threshold is increased to $M \geq 5.0$, and especially $M \geq 6.0$, all aftershocks are located within a few kilometers of the mainshock rupture (Fig. 2). The largest aftershocks tend to be closest to the mainshocks, as has been noted previously at Wenchuan (e.g., Lü *et al.*, 2008; Shi *et al.*, 2009) and other places (e.g., Nanjo and Nagahama, 2000; Chen and Wang, 2012; Tahir *et al.*, 2012), though Eneva and Pavlis (1991) and Doser (1989) found null or opposite cases. One argument for larger aftershocks being located on or near the mainshock rupture might be that is where the longest faults are likely to be. However, in the case of the Wenchuan setting, there are many distant faults with calculated stress increases capable of generating $M \geq 6.0$ earthquakes as can be seen from the pre-2008 catalogs shown in Figure 2.

From an admittedly small sampling, it might be hypothesized that the static stress-based forecast in the Sichuan basin is most effective, or only effective, for higher magnitude aftershocks. Reasons for this might include the following: (1) it may be that high static stresses (≥ 1 bar) tend to be required to trigger large aftershocks, (2) in the Wenchuan case, almost all of the faults nearby the mainshock rupture were calculated to have increased failure stress (Fig. 2), and/or (3) the unknown contributions of dynamic triggering by seismic waves (e.g.,

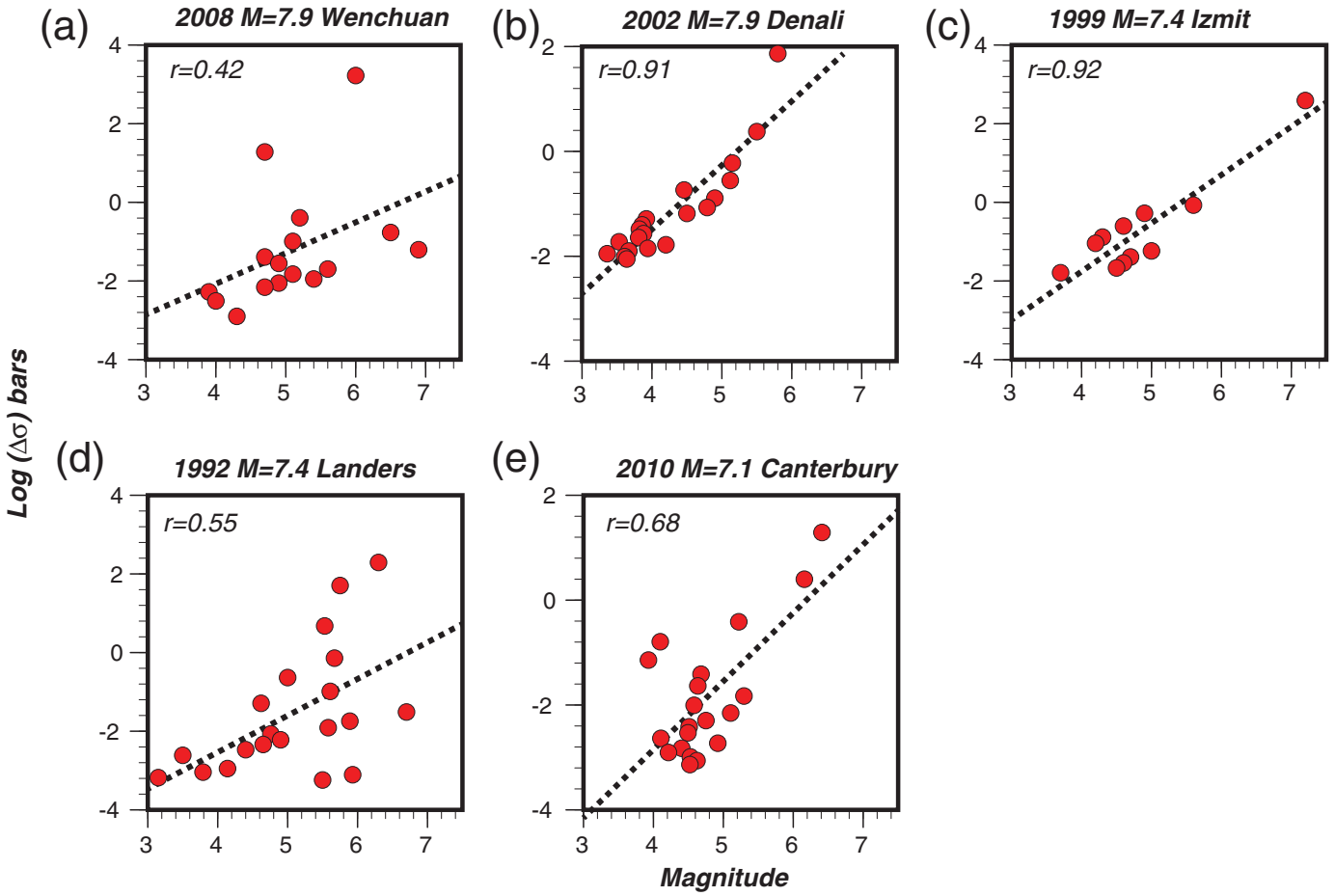

▲ **Figure 4.** Plots show correlations between log stress change and maximum postmainshock magnitudes observed in the same distance ranges as plotted in Figure 3. The −1 value on the vertical axis thus corresponds to the 0.1 bar stress-change threshold. There is a significant relationship between the magnitude of stress change and earthquake magnitude. The correlation coefficients (*r*) are given for each mainshock.

Felzer and Brodsky, 2006; Richards-Dinger *et al.*, 2010) may overprint the static stress-change effect and may only apply to lower magnitude triggered events (Parsons and Velasco, 2011).

From Figure 2 it is also evident that most high-magnitude aftershocks occurred in areas with the highest overall aftershock activity levels (clustering). Therefore the maximum aftershock magnitude may have no direct relationship to the stress change amplitude, but instead may only be a consequence of increased activity. Such clustering behavior forms the basis of highly successful empirical aftershock forecasting methods such as Epidemic Type Aftershock Sequence (ETAS) modeling (Ogata, 1988, 1998).

It would obviously be difficult to settle these often debated points here, but some insight into the generality of observations at Wenchuan can be gained by looking at aftershocks of comparable continental earthquakes. The idea is to see if there is a similar dependence of highest magnitude aftershocks with distance to the mainshock rupture surface and to test correlations between highest calculated static stress change, clustering, and aftershock magnitude.

$M_{max-aftershock}$ VERSUS DISTANCE, MAXIMUM STRESS CHANGE, AND CLUSTERING FOR SELECTED MAINSHOCKS

We examine aftershock and static stress-change characteristics for four additional *M* 7.1 to *M* 7.9 continental earthquakes: the 1992 *M* 7.4 Landers, 1999 *M* 7.4 Izmit, 2002 *M* 7.9 Denali, and 2010 *M* 7.1 Canterbury shocks (Fig. 3). These events were selected because they are in similar settings to the Wenchuan mainshock and have comparable magnitudes and network catalogs. No mainshocks were considered that are not presented here.

We used the following procedure to produce the plots in Figure 3: (1) We simplified the ruptures to a single plane and calculated distances from those planes to every aftershock from a five-year period (except the Canterbury event, which has an approximately three-year duration). (2) We find the maximum aftershock magnitude ($M_{max-aftershock}$) in 20 km distance bins between 0 and 500 km. (3) We calculated static Coulomb stress change from each rupture, resolved on optimally oriented planes using a friction coefficient of $\mu = 0.4$, and tectonic

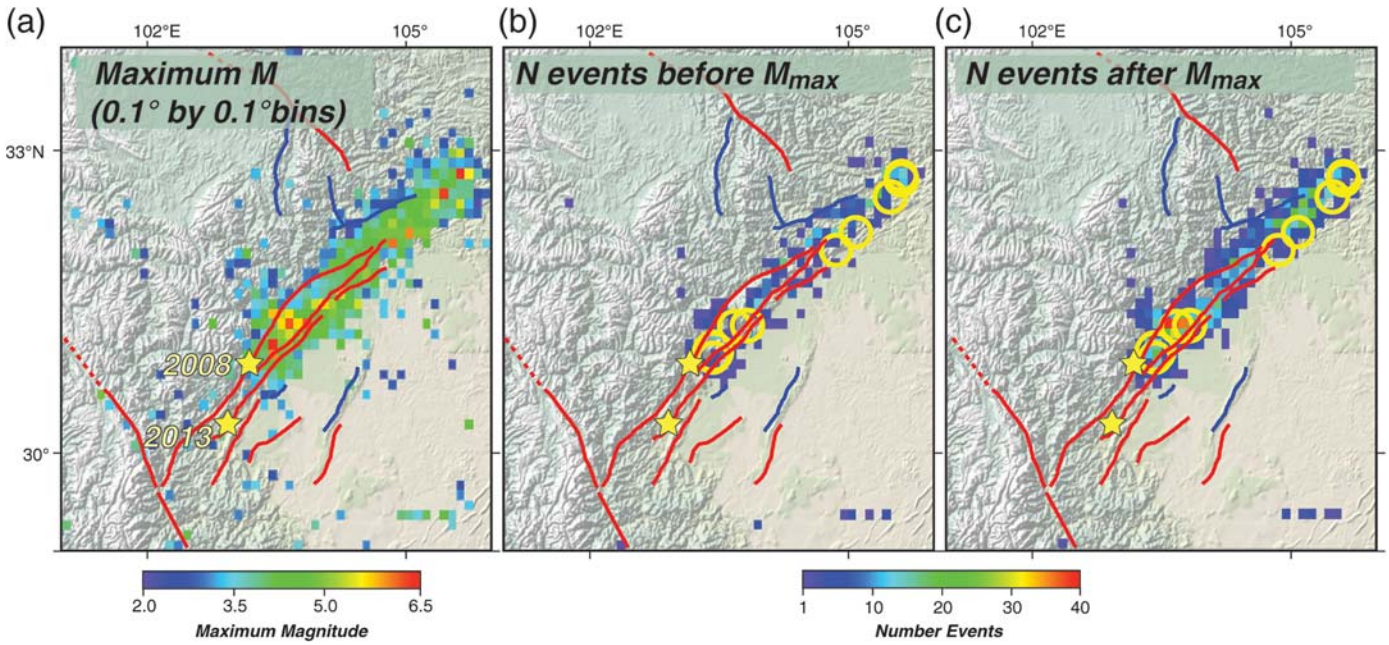

▲ **Figure 5.** Maps showing (a) maximum aftershock magnitudes in 0.1° × 0.1° spatial bins during the five years following the 2008 M 7.9 Wenchuan mainshock, (b) the number of aftershocks preceding the $M_{\text{max-aftershock}}$ in each bin, and (c) the number of events following the $M_{\text{max-aftershock}}$. The yellow circles show the locations of $M \geq 6.0$ aftershocks. Note the lack of prior activity near the 2013 M 6.6 Lushan earthquake.

stress orientations taken from the mainshocks. (4) We found the maximum Coulomb stress increase in the same 20 km distance bins as $M_{\text{max-aftershock}}$ determinations. (5) We calculated the expected maximum aftershock magnitude by linear extrapolation of the Gutenberg–Richter relations ($\log(N) = a - bM$, with b-values from 0.8 to 1.2 and a-values taken from observed rates) of aftershocks in the 20 km distance bins. (6) We used the ~20-year premainshock catalogs to find the maximum observed magnitudes in the same distance bins to gain insight into what magnitudes might be possible versus distance. (7) As a guideline, we then calculated the distance range from mainshock ruptures where the mean aftershock seismicity rate (events per year) is higher than the premainshock mean.

The purpose for making these calculations is to compare the generalized distance reach of the static stress increase and activity levels (clustering) with $M_{\text{max-aftershock}}$ values for a number of different earthquakes so as to establish whether there is a consistent trend that is similar to the observations plotted in Figure 2. The Coulomb stress calculations are subject to parameter uncertainty that affects the specific mapped patterns of stress change. In this instance the primary feature of interest is an expression and comparison of the falloff of maximum stress change versus distance in a general way. Therefore the details of the calculations are less important than uniformity of approach for each event.

From the resulting plots it is clear that the maximum aftershock magnitudes tend to occur closest to the mainshock ruptures and decay with distance (Fig. 3). For most of the mainshocks, the slope of $M_{\text{max-aftershock}}$ falloff is steepest in the first 100 km away from mainshock ruptures. This change in slope is also associated roughly with the range of postmainshock seismicity rate increase and the 0.1 bar maximum stress change increase that has been suggested as a minimum necessary to cause triggering (e.g., Reasenberg and Simpson, 1992; Hardebeck *et al.*, 1998; Harris, 1998). This can be interpreted as a static stress-change process operating across an approximately 80–200 km distance from mainshock ruptures with highest magnitude aftershocks corresponding to highest stress changes.

The apparent correlations between calculated Coulomb stress magnitude and $M_{\text{max-aftershock}}$ in Figure 3 can be quantified if the log maximum stress-increase values versus distance from the mainshock rupture plane are compared with the maximum magnitude aftershocks versus distance. The distance binning is retained because it provides a means of isolating the maximum magnitude events. There is a significant empirical correlation between log stress change and $M_{\text{max-aftershock}}$ for the investigated mainshocks (Fig. 4), with the correlation coefficient (r) values ranging from 0.42 to 0.92. While there is a defendable general correlation amongst distance, magnitude of stress change, and triggered earthquake magnitude, the observations are noisy enough that applying a higher stress-change threshold than the traditional +0.1 bar value (e.g., Reasenberg and Simpson, 1992; Hardebeck *et al.*, 1998; Harris, 1998) would miss many $M > 5$ aftershocks (Fig. 4). Empirically, however, odds are that most high-magnitude triggered events will be found where stress changes are largest. However, it is also apparent that most triggered events of all magnitudes can be found where stress changes are largest (Fig. 3), and both quantities diminish with distance.

Observed $M_{\text{max-aftershock}}$ values tend to fall within or close to expected ranges calculated from extrapolations of the

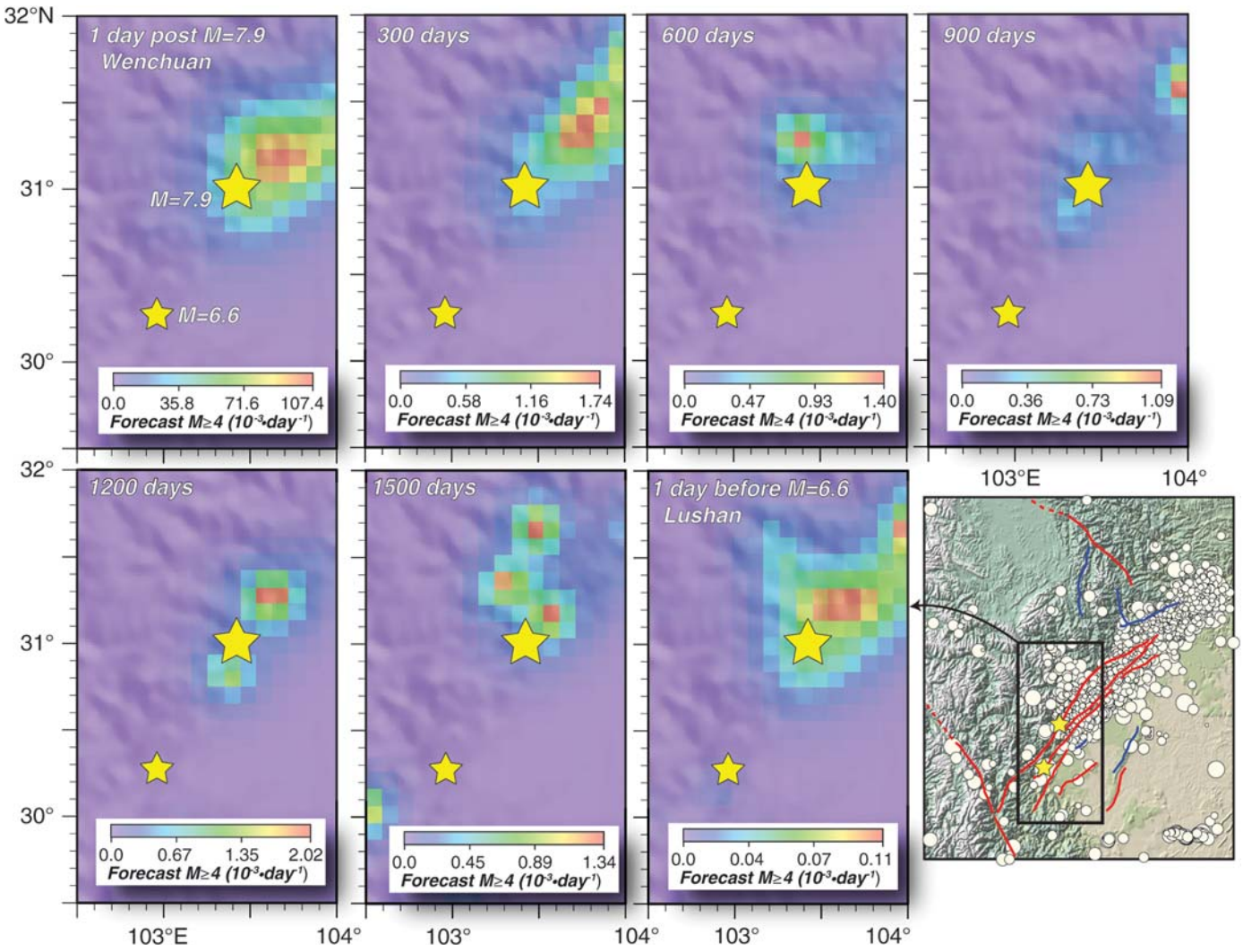

▲ **Figure 6.** Example maps showing 30-day $M \geq 4$ forecast rates in 0.1° × 0.1° spatial bins for different times during the five years following the 2008 M 7.9 Wenchuan mainshock using the time–space ETAS method (Ogata, 1998). Warm colors indicate the highest expected $M \geq 4$ rates; scales are different for each period because of the regional Omori-law decay. At no time after the 2008 mainshock does the location of the 2013 M 6.6 Lushan earthquake show a high expected $M \geq 4$ rate because of the lack of precursory activity as noted in Figure 5. The inset map shows the location of the forecast area.

magnitude frequency distributions of smaller aftershocks (Fig. 3). This raises the question whether the true correlation is between the stress change and $M_{\text{max-aftershock}}$, or instead with the aftershock activity level (a-value); if a Gutenberg–Richter relation applies, then the maximum expected magnitude is a direct function of the a-value. In other words, the actual correlation might be between stress change and aftershock clustering, with higher magnitude events being a byproduct.

To examine the spatial correspondence between activity levels and $M_{\text{max-aftershock}}$ values more closely, we divided the Wenchuan region into 0.1° latitude by 0.1° longitude spatial bins (e.g., Lee *et al.*, 2011) and determined the maximum observed aftershock magnitudes in each bin. We then found the number of events that preceded the maximum magnitude aftershocks (Fig. 5). All but one of the $M \geq 6$ aftershocks (which happens to be the 2013 M 6.6 Lushan event) occurred in areas of elevated prior activity (Fig. 5b). These results typify what is found from empirical forecast methods like ETAS (e.g., Ogata, 1988, 1998; Smyth *et al.*, 2010). In fact, using initial postmainshock activity levels in time–space ETAS models usually outperforms stress-based forecasting in formal evaluations (e.g., Woessner *et al.*, 2011; Segou *et al.*, 2013). However, for the Lushan case, the M 6.6 shock was the first $M > 2$ event to occur in the immediate vicinity (Fig. 5b), and it would thus have been difficult to anticipate from seismicity rate changes in an empirical forecast, as has been shown in Wenchuan and other regions (Fig. 6) (e.g., Shi *et al.*, 2009; Console *et al.*, 2010; Smyth *et al.*, 2010; Werner *et al.*, 2011; Hardebeck, 2013; Segou *et al.*, 2013).

We show sample space-time ETAS (Ogata, 1998) $M \geq 4$ aftershock forecasts from different periods within the interval between the 2008 M 7.9 Wenchuan and 2013 M 6.6 Lushan

Table 1
Maximum Likelihood Estimates of Space-Time ETAS Parameters Used to Forecast $M \geq 4$ Aftershocks in the Wenchuan Region

K (Events/Day/Degree^2)	c (Day)	α (Magnitude^{-1})	P	d (Degree^2)	q	b	Branching Ratio
0.13	0.01	0.8	1.2	0.0071	1.96	1.0	0.57

Parameters K, c, and p are Omori-law values governing the decay rate of aftershocks, α estimates the magnitude efficiency of an earthquake in generating its offspring, d and q are spatial fitting parameters. The parameter b is the Gutenberg–Richter magnitude-frequency slope, and the branching ratio is the estimated number of triggered events per mainshock. See Ogata (1998) for a full discussion.

earthquakes to illustrate the difficulty in anticipating the Lushan earthquake from an empirical basis (Fig. 6). We solved for parameters with a maximum likelihood method (Table 1), and made 30-day forecast calculations at 30-day intervals throughout the period between the two earthquakes. As expected from Figure 5, there was no indication of enhanced likelihood of future $M \geq 4$ events at the Lushan site during any interval (Fig. 6). Thus while empirical methods were very effective in identifying the spatial and temporal distribution of other $M \geq 6$ events, they were limited in the Lushan case by the dearth of prior activity.

DISCUSSION

Does magnitude matter when evaluating a stress-based forecast? Are empirical forecasts always better? Static stress-based methods appear effective for higher magnitude ($M \geq 6$) aftershocks in the Wenchuan region, most notably the interaction between the 2008 M 7.9 mainshock and the 2013 M 6.6 Lushan event. Similarly, the 2010 M 7.1 Canterbury and 2011 M 6.3 Christchurch pairing in New Zealand (Stramondo *et al.*, 2011), and the 1999 M 7.4 Izmit and M 7.2 Düzce shocks in Turkey (Hubert-Ferrari *et al.*, 2000; Parsons *et al.*, 2000) are consistent with static stress-change models. A potential exception is the 1992 M 7.4 Landers and 1999 M 7.1 Hector Mine earthquake pair in California, the hypocenters of which lie about 60 km apart. Parsons and Dreger (2000) suggested the slip distribution of the Hector Mine event was influenced by the stress change from the Landers mainshock, though Harris and Simpson (2002) found most stress-change models did not put the Hector Mine hypocenter in a stress-increased zone. Globally, about 80% of $M \geq 6.0$ aftershocks were found to be consistent with static stress-change calculations using a 20-year centroid moment tensor catalog versus 61% for $M \geq 5.0$ shocks (Parsons *et al.*, 2012).

In contrast, it has been more difficult to correlate static stress-change calculations with the full magnitude spectrum (e.g., Felzer and Brodsky, 2005; Mallman and Zoback, 2007; Hainzl *et al.*, 2009) (Fig. 1). This correlation is very likely complicated by multiple triggering mechanisms in the near field that include the static stress changes discussed here, as well as dynamic triggering by body waves (e.g., Gomberg *et al.*, 1997; Kilb *et al.*, 2000; Felzer and Brodsky, 2006), pore fluid flow (e.g., Nur and Booker, 1972), and viscoelastic stress transfer (e.g., Melosh, 1976; Pollitz and Sacks, 2002).

Because the largest aftershocks are clearly the important ones to forecast correctly, the exercises in this paper point out three (likely not independent) considerations: (1) the most probable places that high-magnitude aftershocks will occur are where there is the highest overall aftershock activity, (2) high-magnitude aftershocks are most likely to happen where stress-change calculations are greatest, and (3) high-magnitude aftershocks are most likely to happen on well-developed fault zones. All three of these points are fairly obvious, but the 2008 M 7.9 Wenchuan and 2013 M 6.6 Lushan pair highlights the devastating importance of exceptions. For example, if the Lushan earthquake is taken to have been correctly forecasted (Figs. 1, 2), then its location was predicted from geology and stress-change calculations only. If forecasting were limited to considering post-2008 clustering, then the Lushan earthquake location would not have been anticipated (Figs. 5, 6). Our conclusion is that stress-based and empirical forecasts have limitations such that both need to be considered.

ACKNOWLEDGMENTS

We thank Eric Geist and Rob Kayen for reviews on an earlier draft and an anonymous reader for *SRL*. We also appreciate the efforts of Editors Zhigang Peng and Huajian Yao in assembling this special section of *SRL*. Figures in this review utilized the Generic Mapping Tool software of Wessel and Smith (1991).

REFERENCES

Chen, K.-C., and J.-H. Wang (2012). Correlations between the mainshock and the largest aftershock for Taiwan earthquakes, *Pure Appl. Geophys.* **169,** 1217–1229, doi: 10.1007/s00024-011-0352-9.

Console, R., M. Murru, and G. Falcone (2010). Probability gains of an epidemic-type aftershock sequence model in retrospective forecasting of $M \geq 5$ earthquakes in Italy, *J. Seismol.* **14,** 9–26, doi: 10.1007/s10950-009-9161-3.

Doser, D. I. (1989). Foreshocks and aftershocks of large ($M \geq 5.5$) earthquakes within the western Cordillera of the United States, *Bull. Seismol. Soc. Am.* **80,** 110–128.

Eneva, M., and G. L. Pavlis (1991). Spatial distribution of aftershocks and background seismicity in central California, *Pure Appl. Geophys.* **137,** 35–61.

Felzer, K., and E. Brodsky (2005). Testing the stress shadow hypothesis, *J. Geophys. Res.* **110,** B05S09, doi: 10.1029/2004JB003277.

Felzer, K. R., and E. E. Brodsky (2006). Decay of aftershock density with distance indicates triggering by dynamic stress, *Nature* **441,** 735–738, doi: 10.1038/nature04799.

Gomberg, J., M. L. Blanpied, and N. M. Beeler (1997). Transient triggering of near and distant earthquakes, *Bull. Seismol. Soc. Am.* **87,** 294–309.

Hardebeck, J. L. (2013). Appendix S–Constraining epidemic type aftershock sequence (ETAS) parameters from the Uniform California Earthquake Rupture Forecast, Version 3 catalog and validating the ETAS model for magnitude 6.5 or greater earthquakes, *U.S. Geol. Surv. Open-File Rept. v. 2013–1165*, 24 pp.

Hardebeck, J. L., J. J. Nazareth, and E. Hauksson (1998). The static stress change triggering model: Constraints from two southern California earthquake sequences, *J. Geophys. Res.* **103,** 24,427–24,437.

Hainzl, S., B. Enescu, M. Cocco, J. Woessner, F. Catalli, R. Wang, and F. Roth (2009). Aftershock modeling based on uncertain stress calculations, *J. Geophys. Res.* **114,** B05309, doi: 10.1029/2008JB006011.

Harris, R. A. (1998). Introduction to special section: Stress triggers, stress shadows, and implications for seismic hazard, *J. Geophys. Res.* **103,** 24,347–24,358.

Harris, R. A., and R. W. Simpson (2002). The 1999 M_w 7.1 Hector Mine, California, earthquake: A test of the stress shadow hypothesis? *Bull. Seismol. Soc. Am.* **92,** 1497–1512.

Hubert-Ferrari, A., A. Barka, E. Jaques, S. S. Nalbant, B. Meyer, R. Armijo, P. Tapponnier, and G. C. P. King (2000). Seismic hazard in the Marmara Sea region following the 17 August 1999 Izmit earthquake, *Nature* **404,** 269–273.

Kilb, D., J. Gomberg, and P. Bodin (2000). Triggering of earthquake aftershocks by dynamic stresses, *Nature* **408,** 570–574.

Kuang, P. (2008). Scientists map potential Sichuan aftershock areas (SciDev.Net), 15 July 2008, http://www.scidev.net/en/news/scientists-map-potential-sichuanaftershock-areas.html?utm_source=link&utm_medium=rss&utm_campaign=en_news (last accessed May 2013).

Lee, Y. T., D. L. Turcotte, J. R. Holliday, M. K. Sachs, J. B. Rundle, C.-C. Chen, and K. F. Tiampo (2011). Results of the regional earthquake likelihood models (RELM) test of earthquake forecasts in California, *Proc. Natl. Acad. Sci. U.S.A.* **108,** 16,533–16,538.

Lü, X., M. Gao, Z. Gao, and S. Mi (2008). Magnitude and distance distribution of strong aftershocks in Sichuan-Yunnan region, *Acta Seismol. Sin.* **30,** 397–404.

Mallman, E. P., and M. D. Zoback (2007). Assessing elastic Coulomb stress transfer models using seismicity rates in southern California and southwestern Japan, *J. Geophys. Res.* **112,** B03304, doi: 10.1029/2005JB004076.

Melosh, H. J. (1976). Nonlinear stress propagation in the Earth's upper mantle, *J. Geophys. Res.* **81,** 5621–5632.

Nanjo, K., and H. Nagahama (2000). Observed correlations between aftershock spatial distribution and earthquake fault lengths, *Terra Nova* **12,** 312–316.

Nur, A., and J. R. Booker (1972). Aftershocks caused by pore fluid flow? *Science* **175,** 885–887.

Ogata, Y. (1988). Statistical models for earthquake occurrences and residual analysis for point processes, *J. Am. Statist. Assoc.* **83,** 9–27.

Ogata, Y. (1998). Space-time point-process models for earthquake occurrences, *Ann. Inst. Stat. Math.* **50,** 379–402.

Parsons, T. (2002). Global Omori law decay of triggered earthquakes: Large aftershocks outside the classical aftershock zone, *J. Geophys. Res.* **107,** 2199, doi: 10.1029/2001JB000646.

Parsons, T., and D. Dreger (2000). Static-stress impact of the 1992 Landers earthquake sequence on nucleation and slip at the site of the 1999 $M = 7.1$ Hector Mine earthquake, southern California, *Geophys. Res. Lett.* **27,** 1949–1952.

Parsons, T., C. Ji, and E. Kirby (2008). Stress changes from the 2008 Wenchuan earthquake and increased hazard in the Sichuan basin, *Nature* **454,** 509–510, doi: 10.1038/nature07177.

Parsons, T., and A. A. Velasco (2011). Absence of remotely triggered large earthquakes beyond the main shock region, *Nature Geosci.* **4,** 312–316, doi: 10.1038/ngeo1110.

Parsons, T., Y. Ogata, J. Zhuang, and E. L. Geist (2012). Evaluation of static stress change forecasting with prospective and blind tests, *Geophys. J. Int.* **188,** 1425–1440, doi: 10.1111/j.1365-246X.2011.05343.x.

Parsons, T., S. Toda, R. S. Stein, A. Barka, and J. H. Dieterich (2000). Heightened odds of large earthquakes near Istanbul: An interaction-based probability calculation, *Science* **288,** 661–665.

Pollitz,, F. F., and S. I. Sacks (2002). Stress triggering of the 1999 Hector Mine earthquake by transient deformation following the 1992 Landers earthquake, *Bull. Seismol. Soc. Am.* **92,** 1487–1496.

Reasenberg, P. A., and R. W. Simpson (1992). Response of regional seismicity to the static stress change produced by the Loma Prieta earthquake, *Science* **255,** 1687–1690.

Richards-Dinger, K., S. Toda, and R. S. Stein (2010). Decay of aftershock density with distance does not indicate triggering by dynamic stress, *Nature* **467,** 583–586, doi: 10.1038/nature09402.

Scholz, C. H. (2002). *The Mechanics of Earthquakes and Faulting*, Cambridge University Press, Cambridge, U.K., 225 pp.

Segou, M., T. Parsons,, and W. Ellsworth (2013). Evaluation of combined physics based and statistical forecast models, *J. Geophys. Res.* doi: 10.1002/2013JB010313.

Shi, P., J. Liu, and Z. Yang (2009). Spatio-temporal point pattern analysis on Wenchuan strong earthquake, *Earthq. Sci.* **22,** 231–237, doi: 10.1007/s11589-009-0231–y.

Smyth, C., J. Mori, and C. Jiang (2010). Model ensembles for prediction of Wenchuan aftershock activity, *Bull. Seismol. Soc. Am.* **100,** 2532–2538, doi: 10.1785/0120090300.

Stramondo, S., C. Kyriakopoulos, C. Bignami, M. Chini, D. Melini, M. Moro, M. Picchiani, M. Saroli, and E. Boschi (2011). Did the September 2010 (Darfield) earthquake trigger the February 2011 (Christchurch) event? *Scientif. Rept.* **1,** Article number 98.

Tahir, M., J.-R. Grasso, and D. Amorèse (2012). The largest aftershock: How strong, how far away, how delayed? *Geophys. Res. Lett.* **39,** L04301, doi: 10.1029/2011GL050604.

Toda, S., J. Lin, M. Meghraoui, and R. S. Stein (2008). 12 May 2008 $M = 7.9$ Wenchuan, China, earthquake calculated to increase failure stress and seismicity rate on three major fault systems, *Geophys. Res. Lett.* **35,** L17305, doi: 10.1029/2008GL034903.

UNICEF China (2013). Lushan earthquake situation report #1, 22 April 2013, 6 pp.

Werner, M. J., A. Helmstetter, D. D. Jackson, and Y. Y. Kagan (2011). High-resolution long-term and short-term earthquake forecasts for California, *Bull. Seismol. Soc. Am.* **101,** 1630–1648, doi: 10.1785/0120090340.

Wessel, P., and W. H. F. Smith (1991). Free software helps map and display data, *Eos Trans. AGU* **72,** 441.

Woessner, J., S. Hainzl, W. Marzocchi, M. J. Werner, A. M. Lombardi, F. Catalli, B. Enescu, M. Cocco, M. C. Gerstenberger, and S. Wiemer (2011). A Retrospective Comparative Forecast Test on the 1992 Landers sequence, *J. Geophys. Res.* **116,** no. B05305, doi: 10.1029/2010JB007846.

Tom Parsons
U.S. Geological Survey
345 Middlefield Road, MS 999
Menlo Park, California 94025 U.S.A.
tparsons@usgs.gov

Margaret Segou
GeoAzur
250 Rue Einstein
Sophia-Antipolis 06560, France